Supporting Information : Surface and epitaxial stresses on supported metal clusters

Rémi Lazzari,*,† Jacek Goniakowski,† Gregory Cabailh,† Rémi Cavallotti,† Nicolas Trcera,‡ Pierre Lagarde,‡ and Jacques Jupille†

Sorbonne Universités, UPMC Univ Paris 06, CNRS UMR 7588, Institut des NanoSciences de Paris, F-75005 Paris, France, and Synchrotron SOLEIL, L'Orme des Merisiers, St-Aubin, BP48, F-91192 Gif sur Yvette, France

E-mail: remi.lazzari@insp.jussieu.fr

Experimental

Experiments have been performed on the LUCIA beamline[1] at synchrotron SOLEIL in an ultra-high vacuum apparatus involving a preparation chamber and a main chamber where X-ray absorption spectroscopy (XAS), Low Energy Electron Diffraction (LEED) and Auger electron spectroscopy could be operated (base pressure a few 10^{-8} Pa). $Al_2O_3(0001)$ surfaces were prepared by high temperature thermal treatment (above 1200 K) under oxygen partial pressure (a few 10^{-4} Pa).[2,3] Surface crystallographic quality and sample cleanliness were checked by LEED and Auger spectroscopy once the sample was transferred to the main chamber. Ag/alumina nanoparticles of various sizes were obtained by thermal evaporation from a well out-gassed crucible at a rate of $\sim$ 0.05 nm/min through the Volmer-Weber growth process. Film growth performed at room temperature was monitored *in situ* and in real-time by Surface Differential Reflectivity Spectroscopy (SDRS) to determine the film morphology as done in refs 3,4 (see also Sect.). The description of the optical setup and the principle of the technique can be found in ref 4. Briefly, the measured quantity is the relative variation of the sample reflectivity in the UV-visible photon range (1.5-4.5 eV). *p*-polarized light was used as its electric field components allow simultaneously probing the dielectric behaviour parallel and perpendicular to the substrate. The incoming light (incident angle of 45°) excites the plasmon resonances (or Mie absorption) in the nanosized silver particles which position and intensity are tremendously sensitive to the morphology.[5,6]

The film thickness was determined via the relative jump of X-ray absorption at the Ag L_3 edge calibrated on a silver film which thickness (3 nm) was obtained by a quartz microbalance measurement. This calibration agreed within 20% with the thickness obtained by SDRS analysis as expected from the linear dependence of the two techniques on the total amount of matter. Compared to the reference work of ref 3, nine films from submonolayer up to 1.1 nm thickness spanning the expected range of aspect ratio variation were analysed to determine bond distances by Extended X-ray Absorption Fine Structure (EXAFS) analysis at the Ag L_3 edge (see Sect.). The incoming X-ray photon flux coming from an undulator was provided by a two-crystal monochromator equipped with Si(111) crystals. It was monitored via the drain current of a 50 nm thick nickel film deposited onto a polyethylene foil. The total elec-

*To whom correspondence should be addressed

†Sorbonne Universités, UPMC Univ Paris 06, CNRS UMR 7588, Institut des NanoSciences de Paris, F-75005 Paris, France

‡Synchrotron SOLEIL, L'Orme des Merisiers, St-Aubin, BP48, F-91192 Gif sur Yvette, France

tron yield from the sample was recorded from 3330 eV to 3530 eV to give the EXAFS signal, several scans being averaged (typically 6 scans with a dwell time of 1 second per point). The EXAFS fine-structure function $\chi(E)$ and its photoelectron wavevector counterpart $\chi(k)$ were analysed with the Athena/Artemis codes.[7]

Numerical simulations

Density Functional Theory (DFT) calculations were performed with VASP (Vienna ab initio simulation package),[8,9] with dispersion-corrected GGA (optB88-vdW)[10,11] exchange-correlation functional to improve the description of adhesion characteristics at the weakly interacting silver/alumina interface. Silver adsorption in the limit of nearly-isolated adatoms was simulated with a single Ag atom per (1×1)-$Al_2O_3(0001)$ surface unit cell. Higher Ag coverage was mimicked by a 3 monolayers thick Ag(111) film in $(\sqrt{3} \times \sqrt{3})R30^\circ \parallel (1 \times 1)$ -$Al_2O_3(0001)$ coincidence with the oxide substrate (4 % lattice mismatch). The Al-terminated alumina(0001) substrate was represented by a slab composed of three -Al/3O/Al- layers, with the in-plane lattice parameters fixed at bulk alumina values and with adsorbates on one side only. The Brillouin zone was sampled with Γ-centred (8×8) Monkhorst Pack grid and the plane-wave cutoff set equal to 400 eV. All atomic positions were relaxed until the residual forces were smaller than 0.01 eV/Å. Atomistic simulations of alumina-supported, nanometre sized Ag particles (up to 10000 atoms and ~ 9 nm of diameter) were performed with Inter-atomic Potentials (IP) for Ag-Ag interaction and a Potential Energy Surface (PES) for the Ag-alumina interaction. Ag-Ag interaction was described by the second moment approximation (SMA) to the tight- binding model,[12–16] with parameters taken from earlier studies.[17,18] The PES representing Ag-alumina interaction has been adjusted to the results of *ab initio* calculations following the approach described in refs 18,19. In the present case, the PES parameters adjusted for adsorption of isolated atoms has been rescaled as to obtain a satisfactory agreement for the adhesion of multilayer Ag deposit. With this energetic model, the motif optimization approach was used to generate closed-shell particles with the lowest excess energy.[18–20]

EXAFS analysis

All x-rays absorption spectra have been recorded beyond the silver L_3 edge by monitoring the total electron yield from the sample, at normal and "almost" grazing incidences (60° off-normal). They have then been analyzed using the Athena/Artemis codes[7] in a way analogous to that of standard K-edges. In other words, the $p \rightarrow s$ transition as compared to the $p \rightarrow d$ one, and the non-centro symmetric character of the clusters deposited onto a flat surface were neglected. The Fourier Transforms (FT) have been applied to $k^3\chi(k)$ raw data, with a Kaiser-Bessel apodisation window spanning from 1 to 6.7 $Å^{-1}$. The back Fourier Transform spans from 1 to 3.8 Å. Fig. 1-a shows the raw data for silver metal, silver oxide and a deposit of thickness $\sim$ 0.24 nm at normal incidence. Note the different y-scale (right) for the deposit. This comparison evidences the high quality of the data recorded on these very thin overlayers. Fig. 1-b compares the normal and grazing incidence $\chi(k)$ data for the deposit shown in Figure 1-a. Obviously the signal to noise ratio decreases going to grazing incidence because the beam has to be horizontally squeezed to fit inside the sample (Figure 1-b). The variation of the Ag-Ag interatomic distance with the deposited thickness has just been obtained by measuring the shift of the Fourier Transform, relative to the value of silver metal. Nevertheless, for the thinner samples and at grazing incidence, the data evidence the cluster-substrate interaction, as a marked difference between the two polarizations (Figure 2-b). The modulus of the Fourier Transforms of the model compounds and of the 0.24 nm thick deposit at grazing incidence are shown in Figure 1 of the article. The FT of the deposit is splitted into two components: the one around 2.5 Å can be associated to the Ag-Ag distance,

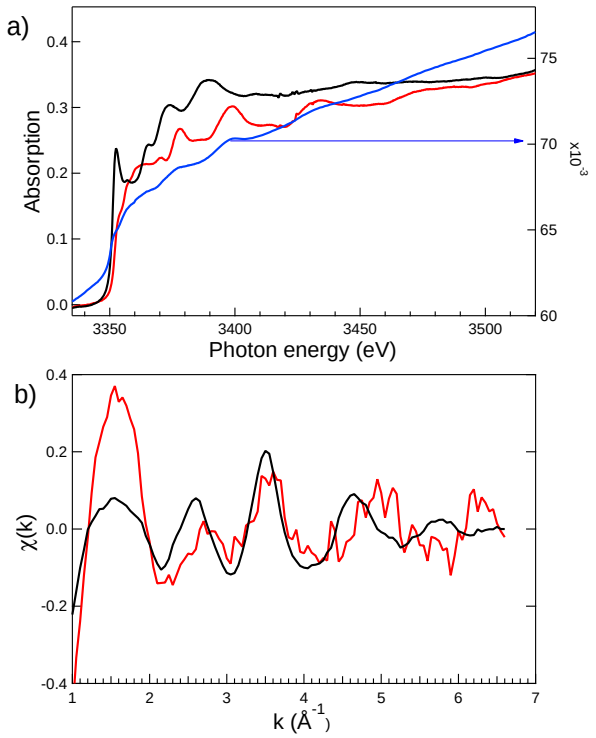

Figure 1: (Color online). EXAFS analysis : (a) Raw data from bulk silver (red line, left scale), silver oxide (black line, left scale) and 0.24 nm thick deposit on alumina (blue line, right scale); (b) $\chi(k)$ data for one monolayer (0.24 nm) of Ag/alumina, as analyzed at normal (black line) and grazing (red line) incidence.

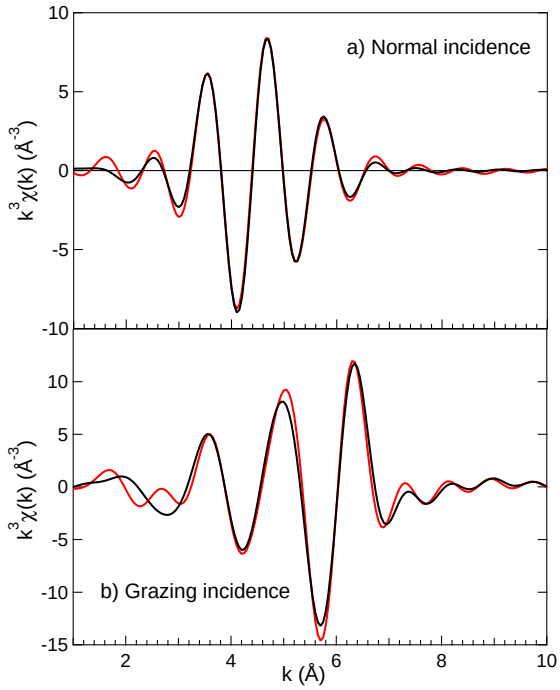

Figure 2: (Color online). EXAFS analysis : Fourier transforms of data (black curve) and corresponding simulations (red curves) for very small silver clusters (film thickness 0.04 nm) at a) normal incidence and b) grazing incidence.

while the shoulder at smaller R values arises from aluminium or oxygen neighbours of the alumina surface. Then a numerical analysis (Artemis) made use of phase shifts of Ag-Ag and Ag-O from a FEFF calculations[21] applied to pure silver metal and pure silver oxide structures respectively, while Ag-Al are extracted from an *ad hoc* cluster where a silver atom is surrounded by 8 Al at 2.55 Å. This fitting procedure returns an Ag-O distance around 2.65 ± 0.05 Å and definitely excludes any occurrence of Ag-Al pairs. The value obtained for Ag-Ag in the case of a 1ML deposit is 2.83 Å, in line with the direct measurement described above. Applied to the normal incidence data, the same analysis cancels the oxygen contribution, a result which is also obtained, whatever the polarisation, for larger clusters. A comparison between experiment and theoretical fit is shown in Figure 2 for the two polarisations and for small clusters.
Grazing measurements show clearly the signature of a well defined site of anchoring of the interfacial silver atoms to the surface, while this contribution vanishes on the EXAFS data for large clusters by a simple renormalisation effect on the number of probed silver atoms.

SDRS analysis

Particle morphology was derived from the analysis of SDRS spectra in the framework of the surface susceptibilities[22–24] by modeling particles with truncated spheres.[22,25,26] Extensive description of the foundation of this dielectric approach, of all numerical technical details and a discussion on the $Ag/Al_2O_3(0001)$ growth process can be found in refs 3,4,27 (and references therein). The soundness of this plasmonic characterization of particle morphology was demonstrated over the past years in several ways. It allowed (i) pinpointing the geometric nature of the plasmon resonances in metallic supported clusters[23,24,28,29] whatever the substrate or the metal, (ii) characterizing wetting at the nanoscale from particle aspect ratio determination[2,3,24,30] and (iii) discussing in details the physics of metal/oxide growth[3,23,27] in a comparable way to Grazing Incidence Small Angle X-Ray Scattering.[30–32]
On an optical point of view, film morphology was modeled herein by truncated spheres on an hexagonal array. The spectra were fitted with 5 free parameters, namely particle diameter or size D, particle truncation $1 + t_r$ *i.e.* height/radius, inter-particle distance L and inhomogeneous effective broadening $\sigma_{\parallel}, \sigma_{\perp}$ to account for size/shape distribution.[3,4,27] Particle contact angle $\theta_c = -\arccos(t_r)$, density $\rho = 2/\sqrt{3}L^2$ and average film thickness (or optical thickness) $t = \pi\rho D^3(2/3 - \cos\theta_c - \cos\theta_c^3/3)$ could be derived easily from the latter. Those parameters are representative of the average growing object.

Figure 3-a shows the best agreement achieved between experimental spectra and modeling for the nine samples which have been analysed by EXAFS. Fits were performed through non-linear least-squared minimization[33] and error bars obtained from χ^2 curvature at the minimum. A comparison is also given with fits performed all along the growth process on a given sample (Figure 3-b). The results of the analysis regarding the film morphology D, ρ, θ_c are gathered in Figures 4. The comparison to previous works[3,4] demonstrate the robustness of the overall trends and of the sensitivity of the optical measurement to nucleation, growth and coalescence stages. In particular, the decrease of contact angle and therefore of the increase of adhesion below 5 nm in size is well reproduced and parallels the molecular dynamics simulations. Fluctuations of parameters from one sample to the other may be explained by the sensitivity of the growth process on the initial number of defects, and therefore on nucleation sites of the surface, on the evaporation rate as well as on the actual achieved temperature after sample preparation and cooling. The last point (circle-cross) of θ_c (Figure 4-b) used in Figure 3-a,b of the article was extrapolated from XAS thickness and size evolution of a sample which parameter was determined from EXAFS; it corresponds to the equilibrium contact angle as measured by mascroscopic sessile drop technique.[34] Finally, values of inhomoge-

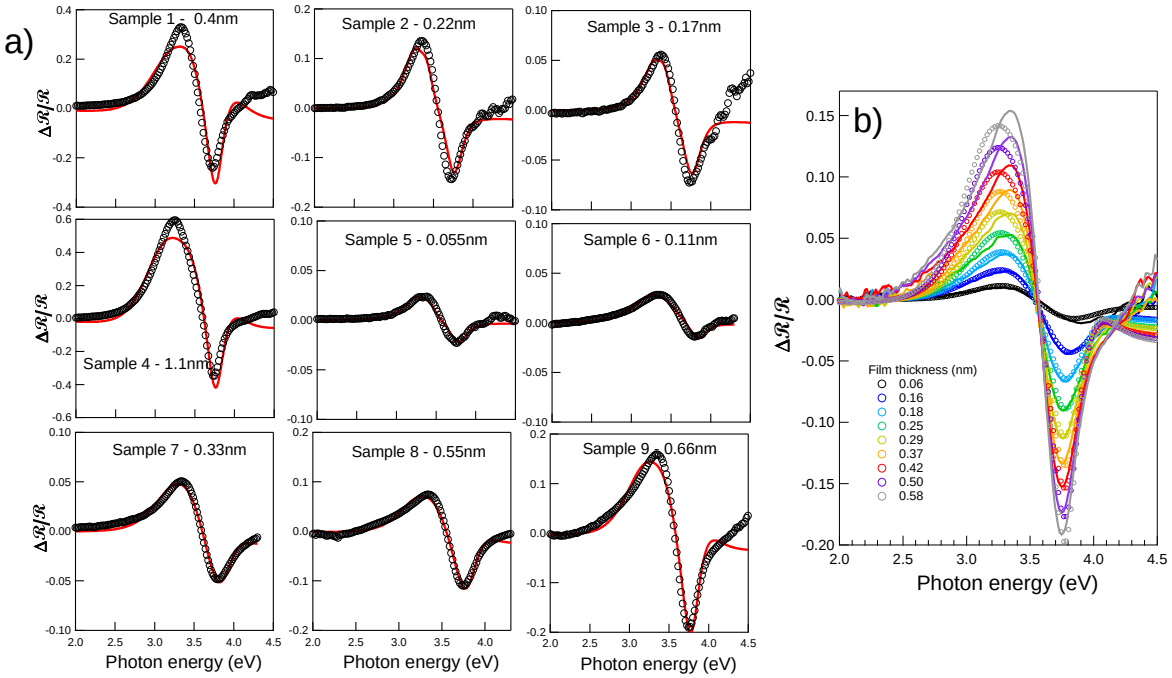

Figure 3: (Color online). SDRS analysis of $Ag/Al_2O_3(0001)$ films : a) Fits (lines) of the spectra (points) at the end of the growth for the nine samples simultaneously characterized by EXAFS. b) Evolution of SDRS spectra and their fits along a given growth process (sample 9). Film thickness as obtained by XAS calibration is given on figures.

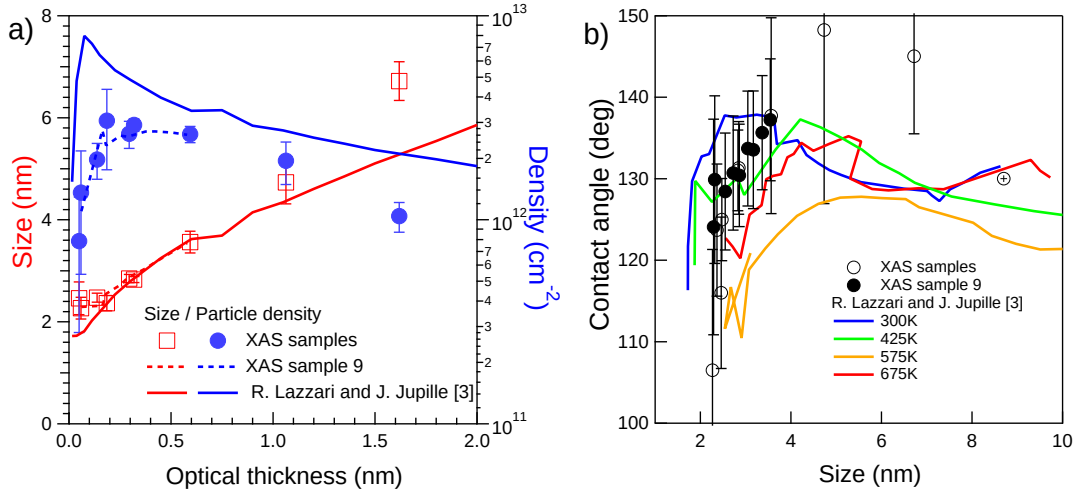

Figure 4: (Color online). $Ag/Al_2O_3(0001)$ cluster morphology from SDRS : a) Size D and density ρ and b) contact angle θ_c obtained from optical fits. Results are compared to the values of ref 3.

neous broadening (not shown) turned out to be very similar to those of ref 3,4 ($\sigma_{\parallel} \simeq 0.2$ eV; $\sigma_{\perp} \simeq 0.1$ eV).

References

(1) Flank, A.-M.; Cauchon, G.; Lagarde, P.; Bac, S.; Janousch, M.; Wetter, R.; Dubuisson, J.-M.; Langlois, F.; Idir, M.; Moreno, T.; Vantelon, D. *Nuclear Instruments and Methods B* **2006**, *246*, 269–274.

(2) Lazzari, R.; Jupille, J. *Phys. Rev. B* **2005**, *71*, 045409.

(3) Lazzari, R.; Jupille, J. *Nanotechnology* **2012**, *23*, 135707–135720.

(4) Lazzari, R.; Jupille, J. *Nanotechnology* **2011**, *22*, 445703.

(5) Kreibig, U.; Vollmer, M. *Optical Properties of Metal Clusters*; Springer Series in Material Science, Springer Verlag: Berlin, Germany, 1995; Vol. 25.

(6) Bohren, C. F.; Huffman, D. R. In *Absorption and Scattering of Light by Small Particles*; Wiley-Interscience,, Ed.; John Wiley & Sons: New York, 1983.

(7) Ravel, B.; Newville, M. *J. Synchrotron Rad.* **2005**, *12*, 537.

(8) Kresse, G.; Furthmüller, J. *Phys. Rev. B* **1996**, *54*, 11169–11186.

(9) Kresse, G.; Hafner, J. *Phys. Rev. B* **1993**, *47*, 558.

(10) Dion, M.; Rydberg, H.; Schroder, E.; Langreth, D. C.; Lundqvist, B. I. *Phys. Rev. Lett.* **2004**, *92*, 246401.

(11) Klimes, J.; Bowler, D. R.; Michaelides, A. *Phys. Rev. B* **2011**, *83*, 195131.

(12) Pettifor, D. *Bonding and structure of molecules and solids*; Oxford University Press, 1995.

(13) Finnis, M. *Interatomic Forces in Condensed Matter*; Oxford University Press, 2003.

(14) Cyrot-Lackmann, F.; Ducastelle, F. *Phys. Rev. B* **1971**, *4*, 2406–2412.

(15) Gupta, R. P. *Phys. Rev. B* **1981**, *23*, 6265–6270.

(16) Rosato, V.; Guilloppé, B.; Legrand, B. *Philos. Mag. A* **1989**, *59*, 321.

(17) Ouahab, A.; Mottet, C.; Goniakowski, J. *Phys. Rev. B* **2005**, *72*, 035421.

(18) Ferrando, R.; Rossi, G.; Levi, A.; Kuntova, Z.; Nita, F.; Jelea, A.; Mottet, C.; Barcaro, G.; Fortunelli, A.; Goniakowski, J. *J. Chem. Phys.* **2009**, *130*, 174702.

(19) Vervisch, W.; Mottet, C.; Goniakowski, J. *Phys. Rev. B* **2002**, *65*, 245411.

(20) Olander, J.; Lazzari, R.; Mangili, B.; Goniakowski, J.; Renaud, G.; Jupille, J. *Phys. Rev. B* **2007**, *76*, 075409.

(21) http://feffproject.org/.

(22) Bedeaux, D.; Vlieger, J. *Optical Properties of Surfaces*; Imperial College Press: London, 2001.

(23) Lazzari, R.; Simonsen, I.; Jupille, J. *Plasmonics* **2014**, *9*, 261–272.

(24) Lazzari, R.; Jupille, J.; Cavallotti, R.; Simonsen, I. *J. Phys. Chem. C* **2014**, *118*, 7032–7048.

(25) Simonsen, I.; Lazzari, R.; Jupille, J.; Roux, S. *Phys. Rev. B* **2000**, *61*, 7722–7733.

(26) Lazzari, R.; Simonsen, I.; Bedeaux, D.; Vlieger, J.; Jupille, J. *Eur. Phys. J. B* **2001**, *24*, 267–284.

(27) Grachev, S.; de Grazia, M.; Barthel, E.; Søndergård, E.; Lazzari, R. *J. Phys. D: Appl. Phys.* **2013**, *46*, 375305–375315.

(28) Lazzari, R.; Roux, S.; Simonsen, I.; Jupille, J.; Bedeaux, D.; Vlieger, J. *Phys. Rev. B* **2002**, *65*, 235424–1.

(29) Lazzari, R.; Simonsen, I.; Jupille, J. *Europhys. Lett.* **2003**, *61*, 541–546.

(30) Lazzari, R.; Renaud, G.; Revenant, C.; Jupille, J.; Borenstzein, Y. *Phys. Rev. B* **2009**, *79*, 125428.

(31) Revenant, C.; Renaud, G.; Lazzari, R.; Jupille, J. *Phys. Rev. B* **2009**, *79*, 235424.

(32) Renaud, G.; Lazzari, R.; Leroy, F. *Surf. Sci. Rep.* **2009**, *64*, 255–380.

(33) Press, W. H.; Teukolsky, S. A.; Vetterling, W. T.; Flannery, B. P. In *Numerical Recipes in Fortran*; Press, C. U., Ed.; Cambridge University Press, 1992.

(34) Chatain, D.; Chabert, F.; Ghetta, V.; Fouletier, J. *J. Am. Ceram. Soc.* **1994**, *77*, 197–201.

Acknowledgement This work benefited from the technical support of D. Roy (SOLEIL), S. Chenot (INSP) and H. Cruguel (INSP). R. Cavallotti PhD thesis was supported by a CIFRE grant form Arcelor-Mittal company.